Journal of
Microscopy

Journal of Microscopy, Vol. 250, Issue 3 2013, pp. 166–178
Received 8 December 2012; accepted 26 February 2013

doi: 10.1111/jmi.12032

An automatic vision-based malaria diagnosis system

J.P. VINK*, M. LAUBSCHER†, R. VLUTTERS*, K. SILAMUT‡, R.J. MAUDE‡,§, M.U. HASAN‖ & G. DE HAAN*

**Video and Image Processing Group, Philips Group Innovation, Research, Eindhoven, The Netherlands*

†Applied Chemical Technology Group, Philips Group Innovation, Research, Eindhoven, The Netherlands

‡Mahidol-Oxford Tropical Medicine Research Unit, Faculty of Tropical Medicine, Mahidol University, Bangkok, Thailand

§Centre for Tropical Medicine, CCVTM, University of Oxford, Oxford, UK

‖Department of Medicine, Chittagong Medical College Hospital, Chittagong, Bangladesh

Key words. Computer aided diagnosis, fluorescent microscopy, image analysis, malaria parasites, *Plasmodium falciparum*, supervised learning.

Summary

Malaria is a worldwide health problem with 225 million infections each year. A fast and easy-to-use method, with high performance is required to differentiate malaria from non-malarial fevers. Manual examination of blood smears is currently the gold standard, but it is time-consuming, labour-intensive, requires skilled microscopists and the sensitivity of the method depends heavily on the skills of the microscopist.

We propose an easy-to-use, quantitative cartridge-scanner system for vision-based malaria diagnosis, focusing on low malaria parasite densities. We have used special finger-prick cartridges filled with acridine orange to obtain a thin blood film and a dedicated scanner to image the cartridge. Using supervised learning, we have built a *Plasmodium falciparum* detector. A two-step approach was used to first segment potentially interesting areas, which are then analysed in more detail. The performance of the detector was validated using 5 420 manually annotated parasite images from malaria parasite culture in medium, as well as using 40 cartridges of 11 780 images containing healthy blood.

From finger prick to result, the prototype cartridge-scanner system gave a quantitative diagnosis in 16 min, of which only 1 min required manual interaction of basic operations. It does not require a wet lab or a skilled operator and provides parasite images for manual review and quality control. In healthy samples, the image analysis part of the system achieved an overall specificity of 99.999978% at the level of (infected) red blood cells, resulting in at most seven false positives per microlitre. Furthermore, the system showed a sensitivity of 75% at the cell level, enabling the detection of low parasite densities in a fast and easy-to-use manner. A field trial in Chittagong (Bangladesh) indicated that future work should primarily focus on improving the filling process of the cartridge and the focus control part of the scanner.

Correspondence to: J.P. Vink, Video and Image Processing Group, Philips Group Innovation, Research, 5656 AE Eindhoven, The Netherlands. Tel: +31 40 2741602; e-mail: jelte.peter.vink@philips.com

Introduction

Malaria is a widespread disease caused by parasites of the genus *Plasmodium*. According to the World Health Organization (WHO, 2010b), malaria kills nearly 800 000 people from approximately 225 million infections each year. Globally, 3.3 billion persons are at risk. In sub-Saharan Africa alone, 765 million persons are at risk of malaria. To differentiate malaria from non-malarial fevers, WHO recommends that all cases of suspected malaria are confirmed with a diagnostic test prior to treatment. Thus, patients can obtain appropriate diagnosis and treatment, leading to reduced mortality rates and recovery times. Moreover, the excessive use of antimalarials can be reduced to limit the development of resistance to antimalarial drugs (WHO, 2010b).

Related work

Several methods for diagnosing malaria are available. Important criteria are cost per test, sensitivity and specificity of the method, time per test and the required skill level of the practitioner. Furthermore, quantification of the number of infected red blood cells (RBCs) is important as a prognostic indicator (Frean, 2009).

Manual examination of blood smears through a microscope is currently the 'gold standard' (Tek *et al.*, 2009). In many malaria endemic regions, there are problems with manual

microscopy, namely the lack of skilled microscopists, variation in experience, limited supply of microscopes, poor maintenance of equipment and inadequate quality control (Coleman *et al.*, 2006).

A recognized way of estimating the number of parasites present in 1 μL of a think blood smear is by using a standard value for the number of white blood cells (WBCs) present (i.e. 8 000 WBC μL^{-1}). The number of parasites per 200 WBC seen is counted. Multiplying by 40 gives the number of parasites per microlitre (parasite density). This method is time-consuming. Experienced microscopists reach a detection limit of around 50 parasites μL^{-1}, whereas routine field microscopy generally achieves a higher detection limit (i.e. around 500 parasites μL^{-1}; Moody, 2002).

Polymerase chain reaction (PCR)-based methods have been used since 1990 and have a lower detection limit than microscopy, especially in cases with low parasite densities or mixed infections (Coleman *et al.*, 2006). They are able to detect five parasites per microlitre of blood (Moody, 2002). However, the cost per test is high and takes up to 24 h, which is unacceptably slow for the initial diagnosis of malaria (Moody, 2002).

Dipsticks or rapid diagnostic tests (RDTs; Bell & Peeling, 2006) are a relatively new approach for the diagnosis of malaria. RDTs detect specific antigens produced by the malaria parasites. The presence of the antigen is indicated by a colour change on the strip and does not require skilled interpretation. If in good condition, RDTs have a reliable performance to a level of 200 parasites μL^{-1} (WHO, 2011). However, like most biological tests, RDTs are prone to deterioration from heat and humidity (Bell & Peeling, 2006). Although RDTs offer savings on training and examination time, the relatively high detection limit remains a problem. Moreover, (semi)quantitative data to determine the parasite density are not currently available (Moody, 2002). Finally, following recent treatment with antimalarial therapy RDTs can remain positive for a period after the clearance of malaria parasites (Bell & Peeling, 2006). This can interfere with diagnosis of a subsequent malaria infection in that period.

Currently, there is no cheap, fast[1] and easy-to-use quantitative method able to detect all clinically relevant parasitaemia levels, especially at low parasite densities (i.e. <50 parasites μL^{-1}). PCR-based methods are costly and time consuming, manual examination is not reliable in many cases and RDTs have a higher detection limit than expert microscopy and do not provide a quantitative result.

In this paper, we propose a complete system using a fully automatic, dedicated microscope design. Although a number of vision studies (Toha & Ngah, 2007; Tek *et al.*, 2009; Špringl, 2009; Sio *et al.*, 2007) have addressed the automated diagnosis of malaria, we have found only one study in the literature which also addresses the complete system. Díaz *et al.* (2009) proposed a system based on bright field microscopy. They have created a motorized microscope, which still needs user interaction. They achieved a specificity of 99.7% (at the level of infected RBCs). Assuming 5 million RBCs μL^{-1} blood (McQueen & McKenzie 2004), the proposed system of Díaz *et al.* would have a performance of 15 000 false positive RBCs μL^{-1} blood, which is far too high to be able to reliably detect low parasite densities. Finally, the system requires 9 s to process an image of 102×76 μm^2. This is unacceptable to achieve the desired specificity of 10 parasites μL^{-1} blood, as tens of thousands of images per cartridge would have to be analysed, leading to a computational time of several days.

In this study, we focus on one species (*falciparum*) of the genus *Plasmodium* that causes human infection. *Plasmodium falciparum* is the most lethal of the human malaria parasites. Furthermore, we will mainly focus on the image analysis part of the system.

This paper is organized as follows. In Section 'Creation of vision-based malaria diagnosis', we will explain how to create a cartridge-scanner system for vision-based malaria diagnosis in detail. In Section 'Results', the trained detector and its performance are described. Finally, discussion and conclusions are presented in Section 'Discussion'.

Creation of vision-based malaria diagnosis

Staining

Over 100 years ago, Giemsa's stain was applied for the first time for the diagnosis of malaria. Since then, it received increased attention. Because of its low direct costs (once a microscope has been purchased), its high sensitivity and specificity and its ability to estimate the level of parasitaemia, microscopical examination is currently widely used (Keiser *et al.*, 2002). However, Giemsa staining requires multiple reagents, experienced personal and is labour intensive and time consuming (it typically requires at least 45 min; Keiser *et al.*, 2002).

Alternative stain recipes are being used, like Field stain that significantly reduces the staining time, although it requires drying of samples before and during staining (Houwen, 2002).

An alternative is acridine orange (AO) using fluorescent microscopy. Compared with Giemsa staining, AO has a good diagnostic performance, with high sensitivity and specificity. Moreover, AO staining requires significantly less time. Diagnostic results are available in only a few minutes (Keiser *et al.*, 2002). As we needed a fast method that is able to detect low parasite densities, AO was selected for our study.

Cartridge design

To be able to determine the parasite density, a thin blood film containing a monolayer of RBCs is preferred over a multilayer thick blood film (Moody, 2002). We used the cartridge as proposed by Camps *et al.* (2012) in which a thin blood film is

[1] As a user requirement, we require that the analysis should be done within 15 min.

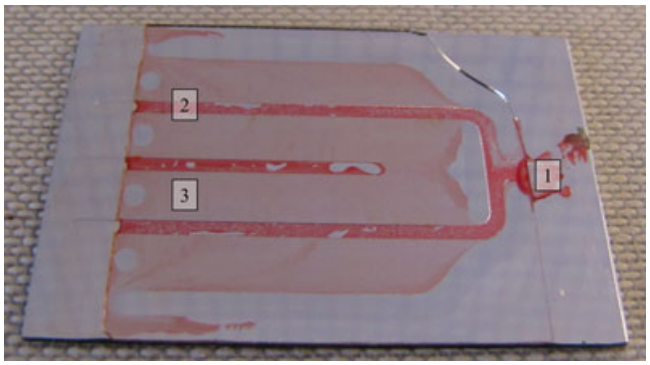

Fig. 1. Cartridge filled with blood and AO.

obtained by making use of capillarity forces. A leading design requirement of the cartridge is low-cost mass production.

The cartridges are made of two components: (i) a glass base plate with the dimensions of half a microscope slide in which channels of 15 μm depth have been manufactured and (ii) a 0.3-mm-thick cover glass. The base plate is coated with an aluminum reflective layer to (i) enhance the fluorescence excitation of the sample and (ii) act as a reference reflection layer for the auto-focus system (discussed in the next section). The two components are assembled and fixed with glue in a semi-automatic process. To assure the required depth, spacer spheres of 3 μm diameter are used to separate the glass base plate and the cover glass. Before usage, cartridges are filled with ethanol-dissolved AO dye and left to dry.

A drop of blood is deposited at the entrance of the cartridge (see [1] of Fig. 1). The blood enters according to capillarity forces in the channels (see [2] of Fig. 1) and consecutively, for smaller parts (e.g. RBC, parasites) in the shallow fields produced by the spacers (see [3] of Fig. 1). The time from depositing the blood drop to a full, stained thin film spread is about 30 s. The dimensions were chosen such that 0.5 μL of blood can be imaged in the four shallow fields. The blood is imaged while it is still liquid, so no waiting time is needed for drying. The cartridges eventually dry in ~4 h in the current design, requiring the imaging to take place within that time period. If needed, the cartridges can be sealed after filling, enabling longer storage times before imaging.

Image acquisition

As indicated above, for the diagnosis of malaria a fast scanner imaging a cartridge within 15 min is required. The first step to achieve this is by using LED illumination. Due to the higher illumination intensity at the sample, more fluorescent signal is obtained. This enabled the use of a low-cost machine vision colour camera (uEye 1220-C from Imaging Development Systems GmBH, Obersulm, Germany) with an exposure time of 20 ms and a frame rate up to 50 Hz (on a static sample).

The second step is to ensure that every image is taken at a unique *XY* position. This requires a sample stage speed of

Table 1. The system properties of the cartridge scanner.

Camera properties	
Number of pixels	752 × 480
Pixel size	6.0 (μm)
Sensor size	4.5 × 2.9 (mm)
Optics properties	
Focal length tube lens	140 (mm)
Magnification	31
Field of view	145 × 93 (μm)
Stage properties	
Stage velocity	3.6 (mm/s)
Scan Area	15.0 × 12.0 (mm)

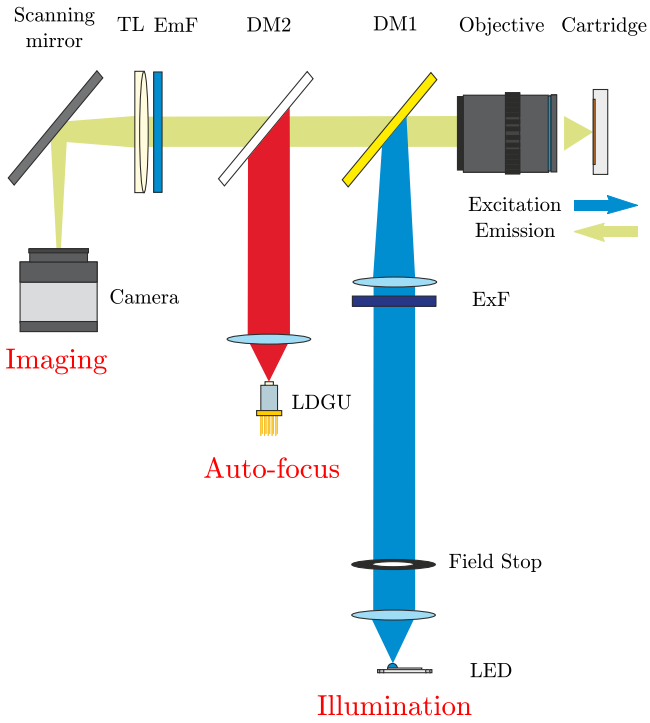

Fig. 2. Schematic design of light-path of malaria scanner.

145 μm at 25 Hz, which is 3.6 mm s^{-1} (see Table 1). At these speeds, it is not optimal to move and stop between every camera image. Therefore, the cartridge is moved with constant speed in *XY* direction, and a scanning galvo mirror was added in the light-path to prevent motion blur. This mirror counter-moves the object image during the exposure time, resulting in a static image on the camera sensor.

Finally, every image is focused by using a laser-based auto-focusing method, similar to a CD player (Stan, 1998). In order for this to work, an aluminum reflective layer has been added to the cartridge. A focus error signal is obtained and fed to a proportional-integral-derivative controller loop to control the *z*-position of the sample stage.

A schematic drawing of the light-path of the built malaria scanner is shown in Figure 2. As can be seen, the sample is

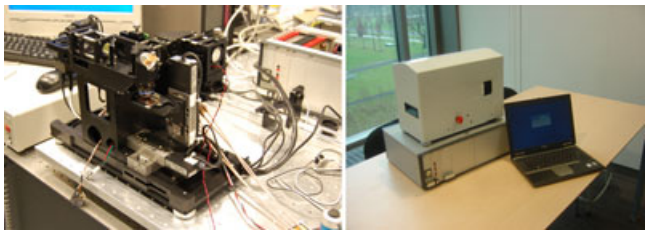

Fig. 3. Left-hand side: the dedicated scanner to image the cartridges. Right-hand side: the microscope scanner, an electronics box and a laptop running Labview.

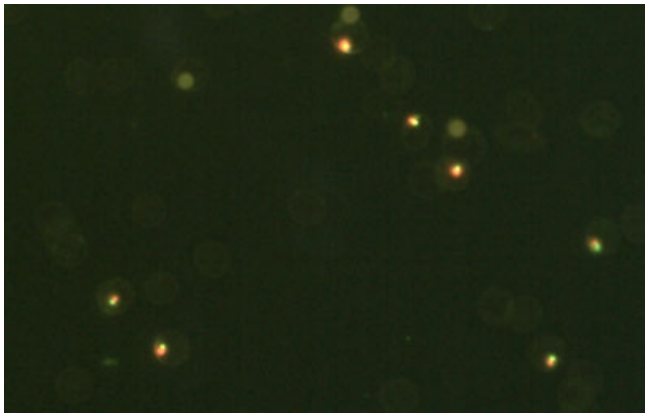

Fig. 4. Image of a digitized glass slide of malaria culture in medium. Multiple infected RBCs are visible. To improve the visibility, we applied some additional contrast boosting.

illuminated with 480 nm light from a Lumiled Rebel Blue and with 780 nm light from a laser diffractive grating unit (LDGU) via an objective lens. Backscattered, reflected and fluorescent light from the cartridge is captured again by the objective lens and goes through the first dichroic mirror (DM1), which lets through all light with a wavelength larger than 500 nm. A second dichroic mirror (DM2) sends all light with a wavelength larger than 700 nm back into the LDGU, and the light in the 500–700 nm range towards the tube lens (TL), the galvo mirror and the camera. An additional filter (EmF) was added behind the tube lens to prevent the excitation light (480 nm) from arriving at the camera.

The main parameters of our system are summarized in Table 1. Using this system, the imaging of one cartridge (0.47 μL whole blood, 11 780 fluorescent images of 752 × 480 pixels with a field-of-view of 145 × 93 μm) takes less than 15 min. In Figure 3, the built malaria scanner can be seen. It consists of the microscope hardware, an electronics box and a PC running Labview (National Instruments Corporation, Austin, USA). A typical example of an image captured by the scanner is shown in Figure 4.

In the next subsection, the image analysis of the digitized images is explained.

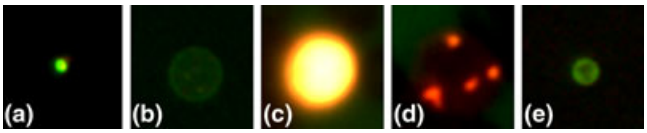

Fig. 5. Typical examples of nonparasites in AO stained blood smear images: (a) platelet (b) RBC (c) WBC (d) reticulocyte (e) spacer. To improve the visibility of the nonparasites, we applied some additional contrast boosting.

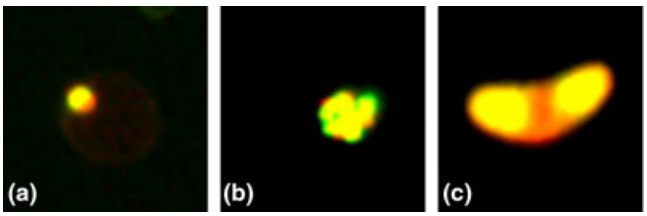

Fig. 6. Typical examples of parasites in AO stained blood smear images: (a) early parasite (b) schizonts (c) gametocyte. To improve the visibility of the malaria parasites, we applied some additional contrast boosting.

Image analysis

The basic property of fluorescent AO staining is that nucleic acids of the parasite strongly fluoresce, whereas the nonparasite containing mature erythrocytes (RBCs) do not contain DNA or RNA and therefore remain mostly unstained as shown in Figure 5 (Keiser *et al.*, 2002). The appearance of a malaria parasite changes substantially through its life cycle in the peripheral blood. Early parasites appear as a single yellow–green coloured nucleus with red fluorescent cytoplasm surrounding it, *rings* appear as a single green nucleus and a rim of red cytoplasm, *trophozoites* have an increasing diameter and an increasing quantity of red cytoplasm as they age and *schizonts* show an increase in the number of green fluorescent nuclei, due to cell division of the chromatin (WHO, 2010a; Hare & Bahler, 1986). Finally, the parasite can develop into a male or female *gametocyte*, recognizable by its round or banana shape (WHO, 2010a) as shown in Figure 6. Besides the parasites, artefacts (e.g. out-of-focus and staining artefacts) also appear in the images as shown in Figure 7. To illustrate the difficulty of recognizing the malaria parasites, 100 parasites and 100 healthy erythrocytes are shown in Figure 8. As can be seen, the healthy erythrocytes can appear similar to the malaria parasites.

In our opinion, there is a small chance that malaria detection can be solved in a purely deterministic way, because of the close resemblance of parasitized erythrocytes to healthy erythrocytes. Therefore, we decided to use machine learning techniques, because of their ability of generalization (Viola & Jones, 2001).

The analysis of the images is time critical. A total of 11 780 images per glass slide have to be analysed in limited time. Because large parts of the images do not contain nucleic acids

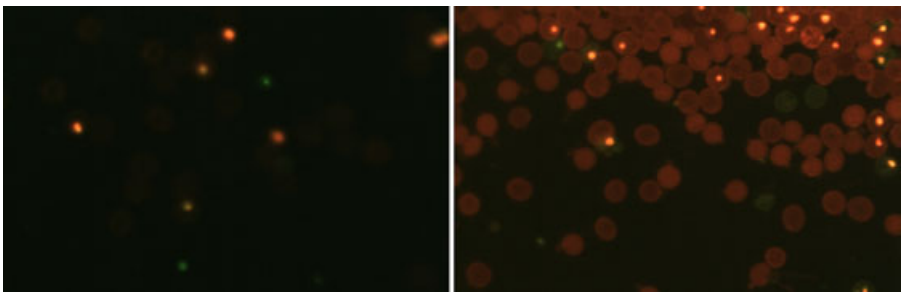

Fig. 7. Image of a digitized glass slide of malaria culture in medium. Left-hand side: out-of-focus artefacts. Right-hand side: staining artefacts.

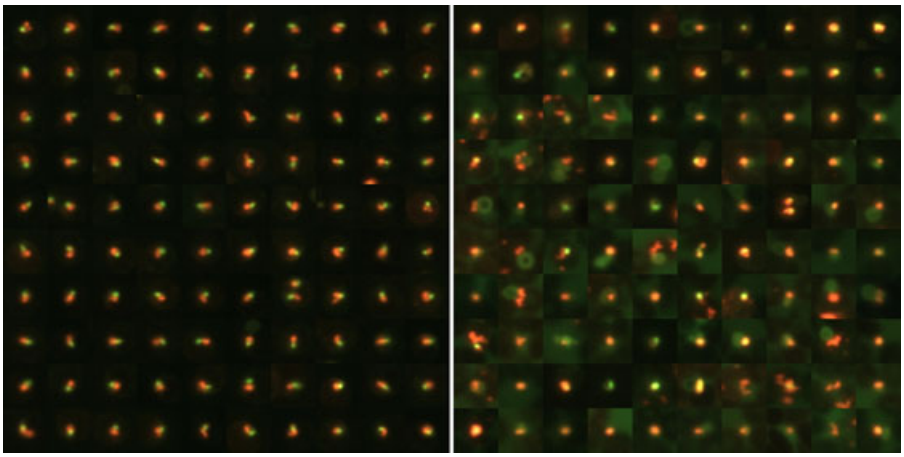

Fig. 8. Left-hand side: examples of malaria parasites from culture in AO. Right-hand side: examples of healthy erythrocytes from peripheral blood.

(DNA or RNA), only the small segments that fluoresce are interesting for further analysis.

Corresponding to the approach of Díaz *et al.* (2009), we used a 2-step approach to increase the throughput. First, the useful segments of an image are determined, which are then classified as parasite and nonparasite. A pixel-accurate classifier is used to segment the image.

Colour plane. The intensity of the images can change due to inevitable variations in sample preparation or dye fabrication (Díaz *et al.*, 2009). Nonetheless, the malaria parasites strongly fluoresce and therefore have a clear contrast with the background. Our fluorescent images contain only noise in the blue channel, as we use fluorescent imaging with AO stain. Therefore, our fluorescent images can be represented in a 2D colour space. In analogy to the colour space HSV used in Díaz *et al.* (2009), we propose to use the colour plane L (intensity) and α (colour)

$$\begin{aligned} \alpha &= \begin{cases} \dfrac{G}{R}, & \text{if R} = \text{MAX} \\ 2 - \dfrac{R}{G}, & \text{if G} = \text{MAX} \end{cases} \\ L &= \text{MAX} \end{aligned} \tag{1}$$

where R and G represent the red and green channel, respectively, and

$$\text{MAX} = \max(\text{R}, \text{G}) \tag{2}$$

α is then defined as the angle in the range [0..2] relative to the contribution of red and green.

Image segmentation

To select the potentially interesting pixels, many local features can be provided, where features are defined as local neighborhood operations applied to an image. To avoid suboptimal, manual selection and thresholding of the local features, we propose to use supervised learning to determine the best feature-threshold combination.

Machine learning. In literature, many supervised learning techniques have been described, although no technique always performs best (Vink & de Haan, 2012). We have not found earlier research proposing machine learning for image segmentation of fluorescent images. Based on the extensive literature study and benchmark of Vink & de Haan (2012), Ada-Boost has shown its potential based on its performance in real-time target detection, its inherent feature selection, its straight-forward use and its low training time. Based on these

findings, we have decided to use Ada-Boost for the segmentation, without claiming it is the best choice.

For the convenience of the reader, the used Ada-Boost variant will be explained in more detail in the next subsection.

Ada-Boost. Ada-Boost creates a strong classifier out of a set of weak classifiers, using a collection of features. In an iterative process, a simple learning algorithm selects the best weak classifier in a greedy process. Data samples are re-weighted to emphasize the incorrectly classified samples.

Formally, using a training data set, Ada-Boost creates a function H that maps pairs of feature values $(\vec{d}_i)$ as inputs to desired outputs or labels (c_i), where

$$\begin{aligned} \vec{d}_i &\in D^M, D \subseteq \mathbf{R}, \\ c_i &\in C = \{-1, 1\}, \\ 0 &\leq i < N, \end{aligned} \tag{3}$$

N represents the number of samples and M the number of feature values per sample.

Ada-Boost establishes a function H

$$H : D^M \rightarrow C \tag{4}$$

that minimizes the error E (Freund & Schapire, 1996)

$$E_H = \sum_{i=0}^{N-1} P(i)\big[c_i \neq H(\vec{d}_i)\big], \tag{5}$$

with respect to distribution $P(i)$. The classifier H is created using the following algorithm (Freund & Schapire, 1997).

Initialize the distribution over the training set $P_1(i) = \frac{1}{N}$
For $t = 1 \ldots T$

1. Train *Weak Learner* using distribution P_t
2. Calculate confidence $\alpha_t \in \mathbf{R}$
3. Update the distribution over the training set:

$$P_{t+1}(i) = \frac{P_t(i) e^{-\alpha_t c_i h_t(\vec{d}_i)}}{Z_t},$$

where Z_t is a normalization factor for distribution P_{t+1}

Final classifier $H(\vec{x})$ is

$$H(\vec{d}) = \begin{cases} 1 & \text{if } \left(\sum_{t=1}^{T} \alpha_t h_t(\vec{d})\right) \geq \Theta \\ -1 & \text{otherwise} \end{cases}$$

where Θ represents a threshold

A cascade of classifiers has been created to achieve increased performance, while reducing the computation complexity (Viola & Jones, 2004). The proposed approach is depicted in Figure 9.

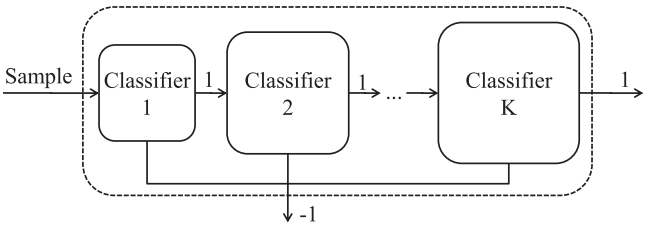

Fig. 9. Schematic depiction of a detection cascade Viola & Jones (2004).

As in Vink & de Haan (2011), a sample $(\vec{d}_i)$ represents a pixel. The desired output (c_i) is a binary label. This is used to indicate if the selected pixel is part of a potentially interesting segment.

For the segmentation, Ada-Boost requires a set of potentially interesting features and a set of labelled samples. In the next subsections, these will be discussed in more detail.

Feature set. The malaria parasites have a clear contrast with the background, due to the applied stain. Therefore, we will focus on features that exploit this property. As thousands of images per cartridge need to be analysed, only a limited amount of time per image is available, which requires features of low computational complexity.

Haar-like (HL) features are used as they are computationally efficient, especially if computed using an integral image (Viola & Jones, 2004). Furthermore, HL features are tolerant to variations, due to the averaging over a rectangular region, and are efficient for representing the image structure of the targeted object (He *et al.*, 2010). We approximate the round or banana shape of the parasites by square Haar-like filters, as a compromise between performance and computational complexity.

Our feature set consists of two types of Haar-like features. First of all, the feature set contains Haar-like box features (He *et al.*, 2010) HL_{W_1,W_2} of image I, where HL_{W_1,W_2} of pixel $\vec{p}_{i,j}$ is defined as

$$\begin{aligned} \mathrm{HL}_{W_1,W_2}(\vec{p}_{i,j}) = {} & SqSum(W_2, \vec{p}_{i,j}) \\ & - \alpha \cdot SqSum(W_1, \vec{p}_{i,j}) \end{aligned} \tag{6}$$

for $W_1 < W_2$, where $SqSum(W, \vec{p}_{i,j})$ is the sum of the pixel-values of a square of size W centered around pixel position $\vec{p}_{i,j}$ of image I (see Fig. 10), α represents the normalization factor, and $\vec{p}_{i,j}$ is defined for an image of (Width $\times$ Height pixels), such that

$$\begin{aligned} 0 &\leq i < \text{Width}, \\ 0 &\leq j < \text{Height}. \end{aligned} \tag{7}$$

Haar-like features can effectively be computed using an integral image (Viola & Jones, 2004). The integral image (II) at pixel position $\vec{p}_{i,j}$ of image I contains the sum of pixel-values

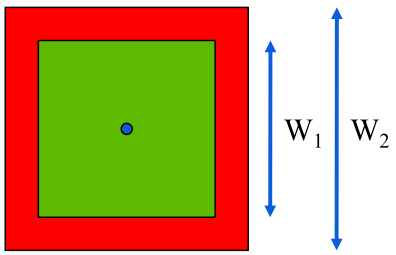

Fig. 10. Haar-like box feature. The blue dot indicates the position of the center pixel. The normalized sum of the pixel-values of the green box is subtracted from the sum of the pixel-values of the red box.

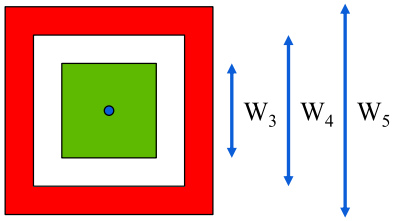

Fig. 11. Non-adjacent Haar-like box feature. The blue dot indicates the position of the center pixel. The normalized sum of the pixel-values of the green box is subtracted from the sum of the pixel-values of the red box.

above and to the left of $\vec{p}_{i,j}$ inclusive and is defined as

$$II(\vec{p}_{i,j}) = \sum_{0\le i'\le i,\ 0\le j'\le j} I(\vec{p}_{i',j'}) \tag{8}$$

This can be calculated recursively, using (Viola & Jones, 2004)

$$\begin{aligned} II(\vec{p}_{i,j}) &= \begin{cases} II(\vec{p}_{i-1,j}) + s(\vec{p}_{i,j}) & \text{if } i \ge 0 \\ 0 & \text{if } i < 0 \end{cases} \\ s(\vec{p}_{i,j}) &= \begin{cases} s(\vec{p}_{i,j-1}) + I(\vec{p}_{i,j}) & \text{if } j \ge 0 \\ 0 & \text{if } j < 0 \end{cases} \end{aligned} \tag{9}$$

in one pass over the original image. Then, *SqSum* can be calculated using only four references to II:

$$\begin{aligned} SqSum(W, \vec{p}_{i,j}) = {} & II(\vec{p}_{i+\lfloor \frac{W}{2} \rfloor, j+\lfloor \frac{W}{2} \rfloor}) + II(\vec{p}_{i-\lfloor \frac{W}{2} \rfloor, j-\lfloor \frac{W}{2} \rfloor}) \\ & - II(\vec{p}_{i+\lfloor \frac{W}{2} \rfloor, j-\lfloor \frac{W}{2} \rfloor}) - II(\vec{p}_{i-\lfloor \frac{W}{2} \rfloor, j+\lfloor \frac{W}{2} \rfloor}). \end{aligned} \tag{10}$$

Besides the Haar-like box features, we also include non-adjacent Haar-like box features, which are claimed to be more efficient and stable (He *et al.*, 2010). Non-adjacent Haar-like box features ($HLNA_{W_3,W_4,W_5}$) of image I are defined as (see Fig. 11)

$$\begin{aligned} HLNA_{W_3,W_4,W_5}(p_{i,j}) = {} & \big(SqSum(W_5, p_{i,j}) - SqSum(W_4, p_{i,j})\big) \\ & - \alpha' \cdot SqSum(W_3, p_{i,j}) \end{aligned} \tag{11}$$

for $W_3 < W_4 < W_5$.

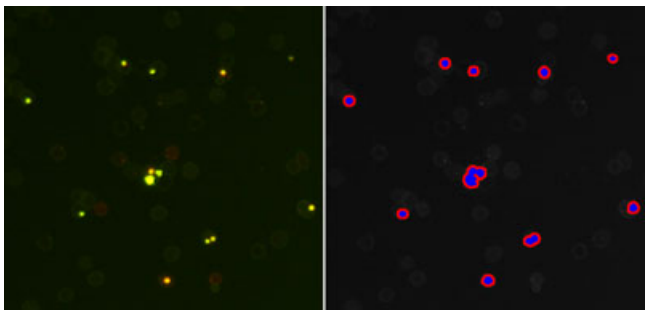

Fig. 12. Part of an image used in the training set for image segmentation. Left-hand side: the original image. Right-hand side: the labelling of the image, where blue represents the potentially interesting pixels, red the pixels which are neglected during training to avoid ambiguous data in the training set, and the black represents the background.

Above features are calculated on L and using the following settings

$$\begin{aligned} 5 &\le W_1 \le 15 \\ 2 &\le W_2 - W_1 \le 16 \\ 5 &\le W_3 \le 15 \\ 2 &\le W_4 - W_3 \le 10 \\ 2 &\le W_5 - W_4 \le 16 \end{aligned} \tag{12}$$

resulting in 528 features.

Training set. Ada-Boost requires two annotated training sets. The first training set is used to select the optimal *Weak Learner*, whereas the second training set determines when to go to the next cascade layer (see Fig. 9). Both training sets are created using 11 images, both selecting randomly 25% of the pixels of each image. The samples are labelled using adaptive (local) thresholding on the brightness channel (Sezgin & Sankur, 2004). Thresholds are manually optimized for each image. An example of an image used in the training set is shown in Figure 12.

Connected component analysis. After establishing the useful pixels, segments are created using connected component analysis (Haralick & Shapiro, 1992). Segments with an area of less than 6×6 pixels are considered as too small and therefore are neglected.

Classification is applied to differentiate between the segments containing malaria parasites and non-malaria segments containing, e.g. platelets, RBCs, WBCs, reticulocytes, the spacers of the cartridge, or (staining) artefacts.

Segment classification

To select the malaria parasites from a large set of segments, many local features can be provided. Ada-Boost is used to create a strong classifier, based on multiple weak classifiers

of thresholded local features. As before, Ada-Boost requires a feature set and a sample set, which will be discussed in the next subsections.

Feature set. The appearance of the malaria parasites in the peripheral blood changes substantially, depending on their life cycle stage. In general, the parasites appear as (a combination of) red and green dots. This property has been used while designing the set of features. The set of features has been categorized into colour features, statistical colour features, region property features and texture features.

Colour features. First of all, features of low computational complexity were included to specify the relative strength of the red channel compared to the green channel within a segment:

$$Count_{>\alpha}(S,\theta) = \#_{\vec{p}_{i,j} \in S}\big[\alpha(\vec{p}_{i,j}) > \theta\big],$$
$$Count_{<\alpha}(S,\theta) = \#_{\vec{p}_{i,j} \in S}\big[\alpha(\vec{p}_{i,j}) < \theta\big], \qquad (13)$$

where S represents the segment, $\alpha(\vec{p}_{i,j})$ the colour-value at pixel location $\vec{p}_{i,j}$ and θ a threshold. We set the threshold to 26 different values, divided over the complete range. The thresholds are equidistantly divided over the range, as α (in analogy to hue) is uniformly distributed over the complete range.

Similar features were included to specify the intensity of the segment:

$$Count_{>L}(S,\theta) = \#_{\vec{p}_{i,j} \in S}\big[L(\vec{p}_{i,j}) > \theta\big],$$
$$Count_{<L}(S,\theta) = \#_{\vec{p}_{i,j} \in S}\big[L(\vec{p}_{i,j}) < \theta\big], \qquad (14)$$

where $L(\vec{p}_{i,j})$ represents the intensity at pixel location $\vec{p}_{i,j}$. As before, the threshold was set to 26 different values, equidistantly divided over the complete range.

Statistical colour features. Next to the colour features, several statistical features were included to capture the colour properties of the segments:

$$Hist_{\alpha}(S,i) = \#_{\vec{p}_{i,j} \in S}\big[b_i \le \alpha(\vec{p}_{i,j}) < b_{i+1}\big],$$
$$Mean_{\alpha}(S) = \frac{1}{|S|} \cdot \sum_{\vec{p}_{i,j} \in S}\big[\alpha(\vec{p}_{i,j})\big],$$
$$Var_{\alpha}(S) = \frac{1}{|S|} \cdot \sum_{\vec{p}_{i,j} \in S}\big[\alpha(\vec{p}_{i,j}) - Mean_{\alpha}(S)\big]^2,$$
$$Min_{\alpha}(S) = \min_{\vec{p}_{i,j} \in S}\big[\alpha(\vec{p}_{i,j})\big],$$
$$Max_{\alpha}(S) = \max_{\vec{p}_{i,j} \in S}\big[\alpha(\vec{p}_{i,j})\big], \qquad (15)$$

where i represents the i^{th} bin of the histogram, bounded by b_i and b_{i+1}, and $|S|$ the cardinality of set S. A histogram consisting of 64 bins was created. Above features were also calculated using the intensity (i.e. L).

Region property features. Multiple region properties were included in the feature set, to include structural information regarding the segments:

$$\text{Area}(S) = |S|,$$
$$Perimeter(S) = \#_{\vec{p}_{i,j} \in S}\big[B(\vec{p}_{i,j})\big],$$
$$Compactness(S) = \frac{Perimeter(S)^2}{Area(S)}, \qquad (16)$$

where $B(\vec{p}_{i,j})$ indicates if $\vec{p}_{i,j}$ is a boundary-pixel of S.

Furthermore, the following region properties have been included[2]:

- $MajorAxis(S)$ and $MinorAxis(S)$: the length of the major and minor axes of the ellipse that has the same normalized second central moments as segment S,
- $FilledArea(S)$: the area of a morphological hole-filled segment S,
- $Eccentricity(S)$: ratio of the distance between the foci of the ellipse and the length of its major axis of segment S,
- $ConvexArea(S)$: the area of the convex hull of segment S,
- $Solidity(S)$: ratio of area of convex hull of segment S and area of segment S.

Texture features. To capture the texture of the segments, the following features have been added (Weszka *et al.*, 1976)[2]:

- $GLCM(S)$: Gray-Level Co-occurrence Matrix, distribution of co-occurring values of neighboring pixels of segment S,
- $Contrast(S)$: intensity contrast between a pixel and its neighboring pixel over the segment S,
- $Correlation(S)$: correlating of a luminance-value of a pixel to its neighboring pixel over the segment S,
- $Energy(S)$: summation of squared elements of $GLCM(S)$,
- $Homogeneity(S)$: closeness of the distribution of elements in $GLCM(S)$ to diagonal of $GLCM(S)$.

In total, the compiled feature set consists of 320 features.

Training set. To train the classifier, multiple cartridges filled with parasite culture in medium were manually annotated in duplicate by experts. A total of 8 413 labelled parasites were randomly divided over the two training sets required by Ada-Boost. A subset of the annotated parasites is shown in Figure 8. As negative samples, 22 cartridges containing healthy blood resulting in 323 312 nonparasite labelled segments out of the

[2] Only a brief description is given, as these features have not been selected by Ada-Boost to detect the malaria parasites.

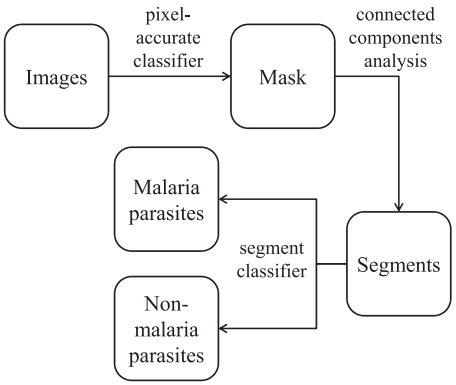

Fig. 13. Framework of the image analysis part to examine the images of a cartridge.

259 160 images were used and also divided over the two training sets. A subset of the negative samples is shown in Figure 8.

Generalization performance. To check for overfitting, the generalization performance was determined. The generalization performance of a trained detector refers to its performance on a test set, which was not part of the set used during training (Jain *et al.*, 2000). In case the detector performed well on the training set, but revealed poor performance on the test set, *overfitting* occurred (Zhou, 2008). The performance of the trained detector depends (among other things) on the proper selection of the number of samples, relative to the number of features. In practice, it is often observed that adding features, while using a small number of samples relative to the number of features in the training set (*curse of dimensionality*), may actually degrade the performance of the detector. This paradoxical behaviour is called the *peaking phenomenon* (Jain *et al.*, 2000). As a rule-of-thumb, it is a good practice to have at least 10 times as many samples per class as the number of features (Jain *et al.*, 2000; Jain & Chandrasekaran, 1982). For our sample set, the number of the positive samples (i.e. the labelled parasites) should therefore have been sufficient to reduce the chance of overfitting.

Framework

In the previous subsections, the automatic, quantitative vision-based malaria diagnosis system was described. After the cartridge has been filled with a drop of blood, images are acquired using a dedicated scanner. Image analysis is applied to examine the images (see Fig. 13). First, the potentially interesting pixels of the images are selected using the pixel-accurate classifier, which has been trained by Ada-Boost. Connected components analysis is applied to create segments. Then, the segments are divided in malaria parasites and non-malaria parasites, based on a detector trained by Ada-Boost.

In the next section, the results of the image analysis part will be discussed.

Results

Image segmentation

Based on the above described framework, we first created the pixel-accurate classifier for the image segmentation. To prevent missed segments and to have a low computational complexity, a conservative cascade consisting of only one layer was built. Only 1 feature was selected by Ada-Boost (i.e. $HLNA_{11,19,35}$). The created pixel-accurate classifier combined with connected components analysis was applied to 1 775 images containing 2 106 parasites to benchmark its performance. Manual inspection of the results indicated that no parasite was missed by the image segmentation.

As expected, a non-adjacent Haar-like feature was preferred over the adjacent Haar-like features, for its robustness and stability. Squares of large size (i.e. 11, 19 and 35) were selected to average over a large area. By that method, noise and artefacts in the images could better be suppressed.

Segment classification

To classify the segments, a second classifier was trained using Ada-Boost. To ensure the required high specificity to be able to detect low parasite densities, the threshold of the last cascade layer Θ was adjusted to accept at most three false positives per cartridge.

Ada-Boost selected the following 10 features (in order of decreasing importance):

- $Count_{>\alpha}(S, 0.625)$,
- $Min_L(S)$,
- $Var_\alpha(S)$,
- $Count_{<L}(S, 0.664)$,
- $Max_L(S)$,
- $Count_{>\alpha}(S, 1.25)$,
- $Compactness(S)$,
- $Hist_\alpha(S, 58)$,
- $Hist_\alpha(S, 57)$,
- $Min_\alpha(S)$.

As already indicated in Section 'Image analysis', the malaria parasites appear as (a combination of) red and green dots. The first three selected features (which are the most important) showed a clear link with the appearance of the parasites. The most important feature $Count_{>\alpha}(S, 0.625)$ indicated that a malaria parasite segment should contain a sufficiently large part that is green or yellow. Combined with the first feature, the third feature $Var_\alpha(S)$ required that a malaria parasite segment also contains a red part. The second feature $Min_L(S)$ required that the malaria parasite segment has sufficient intensity.

The above detector was benchmarked using 40 cartridges containing blood from healthy volunteers (each consisting of 11 780 images) and 5 420 labelled parasite segments, from

Table 2. Computational complexity of the image analysis part of a complete cartridge.

Image segmentation	
Pixel classifier	109.44 *s*
Connected components	87.61 *s*
Segment classification	
Feature calculation	70.07 *s*
Classification	0.18 *s*
Total	267.30 *s*

parasite culture in medium obtained by Radboud University Nijmegen. The image analysis part of the malaria diagnosis system achieved a sensitivity or detection rate (*Pd*) of 75.0%, where *Pd* is defined as

$$Pd = \frac{(\#TP)}{(\#TP) + (\#FN)} \tag{17}$$

using

		Labelled as parasite	
		True	False
Detected parasite	True	True Positives *TP*	False Positives *FP*
	False	False Negatives *FN*	True Negatives *TN*

At most three false positives were found in a cartridge containing healthy blood. On average 0.53 false positives were found in a cartridge containing healthy blood, with a standard deviation of 0.82. As 0.47 μL was scanned per cartridge, this implies that at most 6.38 false positives were found per microlitre blood. By assuming 5 000 000 RBCs per microlitre blood (McQueen & McKenzie 2004), this results in an achieved specificity of 99.999978% at the level of RBCs[3]. Combined with a sensitivity of 75.0%, the image analysis part of our proposed quantitative, automatic vision-based malaria diagnosis system was able to detect low parasite densities (i.e. 10 parasites μL^{-1}) and therefore substantially outperformed proposed alternatives described in the literature.

Timing

The analysis of the images is time critical. Table 2 shows the computational complexity of analysing one complete cartridge, using an Intel dual core processor operating at 3.0 GHz. The images shot by the reader were analysed by the system in less than 4.5 min, amply fulfilling the requirement of performing the analysis within 15 min. The current implementation shows room for improvement to further reduce the computational complexity of the image analysis.

[3] Be aware, this is not the specificity at cartridge level.

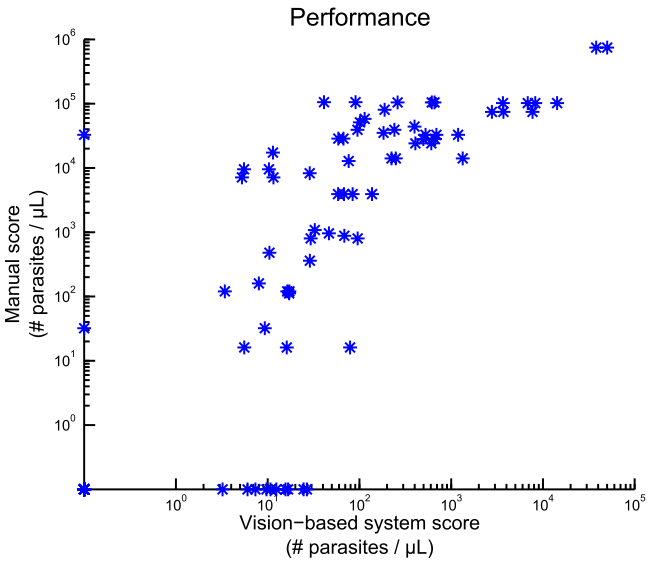

Fig. 14. Result of the field trial, comparing the proposed system to standard microscopy. 14 Samples are clustered in (0,0).

Field trial

To identify points for improvement, the vision-based system was used in a small field trial of hospital inpatients with *Plasmodium falciparum* malaria. The study was performed in Chittagong Medical College Hospital, Chittagong, Bangladesh in July 2011, as part of a wider primary study[4].

The primary study included expert manual microscopy to follow the evolution of enrolled patients' parasite counts with treatment. Discarded blood from the samples taken for microscopy was used to test the proposed system and compared to the manual counts. The results are shown in Figure 14.

Using 86 samples, the proposed system showed a correlation of 0.953 with manual microscopy. However, for two samples no parasites were detected by the proposed system, although otherwise were identified by the manual microscopy. Furthermore, for 10 samples no parasites were found by the microscopist, although were otherwise indicated by the proposed system. Based on these cases, three clear issues have been identified. These issues are out-of-focus artefacts, motion blur and staining artefacts, as shown in Figure 15. As these problems are hard to solve using image processing as a postprocessing step, the causes of these problems should be addressed. Future work should therefore focus on improving the filling process of the cartridges and the auto-focusing system as well as the scanning galvo mirror of the scanner.

[4] 'Malarial retinopathy and near infrared spectroscopy in cerebral and severe malaria', Principal Investigator: Dr. Richard Maude, Mahidol-Oxford Tropical Medicine Research Unit, Mahidol University, Bangkok, Thailand.

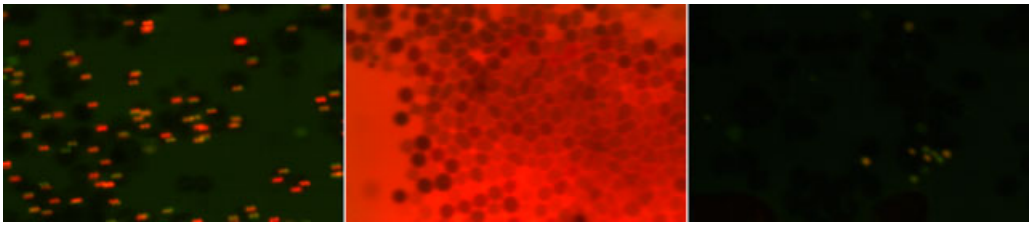

Fig. 15. Examples of a few extreme cases. Left-hand side: motion blur as the sample stage and the scanning galvo mirror were not correctly synchronized. Middle: accumulation of stain resulting in staining artefacts. Right-hand side: out-of-focus image due to an incorrect *z*-position of the sample stage.

Discussion

In this paper, we have proposed a complete system for quantitative, automatic vision-based malaria diagnosis. Manual examination of blood smears is currently the gold standard, but it is time-consuming, labor-intensive, requires a wet lab, requires skilled microscopists and has a detection limit of commonly 500 parasites μL^{-1}, depending on the skill and attention of the microscopist. In favorable conditions, a detection limit of 50 parasites μL^{-1} can be achieved. Dipsticks or RTDs offer savings on training and examination time, but have a higher detection limit of about 200 parasites μL^{-1} and do not allow for quantitative measurements or follow-up.

We selected AO staining as it provides results in minutes and enables a good diagnostic performance. A cartridge, filled with AO, as proposed by Camps *et al.* (2012) was used to obtain a thin blood film. The blood was imaged while still liquid, to eliminate the drying time. Channels of different depths isolated the objects of interest, i.e. RBCs and parasites. A dedicated compact scanner was used to image the cartridges. The scanner comprises a machine vision colour camera, a scanning galvo mirror that prevents motion blur, and a laser-based auto-focus system. The cartridge has an aluminum reflection layer to enhance the excitation and to enable the auto-focus system.

To analyse the images, a high-throughput parasite detector was proposed. We have focused on machine learning strategies, due to the close resemblance of the malaria parasites to healthy erythrocytes. A two-step approach was proposed that first segments the potentially interesting areas, and then classifies the segments. We used supervised learning (Ada-Boost) to train a pixel-accurate classifier to segment the images. Ada-Boost was selected due to its potential shown in Vink & de Haan (2012), without claiming it is the best choice.

To avoid missing segments, a conservative single layer classifier using a single non-adjacent Haar-like feature was created. Haar-like features are attractive as they are computationally efficient and tolerant to variations. The second classifier to analyse the segments in more detail, using the output of the image segmentation, was trained using Ada-Boost and tuned to accept at most three false positives per cartridge, to ensure the required high specificity. This classifier is based on a weighted mixture of only 10 (local) colour and region property features.

The created high-throughput parasite detector was tested on 40 cartridges containing healthy blood, each consisting of 11 780 images and 5 420 segments of labelled malaria parasites. The image analysis part of the system achieved a sensitivity of 75% at the level of (infected) RBCs, while on average 0.53 false positives were found in a cartridge containing healthy blood. At most less than seven false positives per microlitre were found, resulting in a cell-level specificity of 99.999978%.

Vision-based malaria parasite detection has been studied by a number of investigators (Toha & Ngah, 2007; Tek *et al.*, 2009; Špringl, 2009; Sio *et al.*, 2007), but as far as we know, only one study in the literature also addressed the complete system. Díaz *et al.* (2009) proposed a bright field system with Giemsa staining. Although in our proposal, we used fluorescent microscopy combined with AO, the goal of both methods is automatic quantification of malaria parasites in blood. Giemsa stain has the advantage of being used frequently for manual examination, so that microscopists are used to the images. AO requires significantly less time to apply, while still achieving a good diagnostic performance. Díaz *et al.* achieved a specificity of 99.7% and a sensitivity of 94%, based on 450 images consisting of 11 844 healthy RBCs and 713 malaria parasites. Although the sensitivity of the image analysis part of our system was only 75%, our specificity was orders of magnitude higher (i.e. 99.999978%), based on 471 200 images, combined consisting of 94 million RBCs, and 5 420 malaria parasites. Such an extreme high specificity is required to be able to detect low parasite densities.

Preparing the cartridge required less than 1 min. Besides that, the scanning time of a cartridge took less than 15 min and the analysis of images less than 5 min. Because scanning and analysis can run in parallel, the set user requirement was met.

Currently, the scanning time of a cartridge is the bottleneck of the system. Future work will therefore focus on reducing the scanning time.

Compared to the proposed system of Díaz *et al.*, our system is orders of magnitude faster as they require 9 s per image leading to a computational time of multiple days, as tens of thousands of images per cartridge have to be analysed to achieve the desired specificity of 10 malaria parasites μL^{-1}.

The above performance has been achieved on malaria parasites from culture in medium. To identify points for improvement, a small field trial was performed in Chittagong (Bangladesh). Based on 86 samples, the proposed system showed a correlation of 0.953 with manual microscopy. Based on this field trial, issues have been identified with the filling process of the cartridge, the auto-focusing system and the scanning galvo mirror.

In the performed field trial, manual microscopy was used as reference. However, as the detection limit of the 'gold standard' is limited, future field studies should use techniques with a lower detection limit, such as PCR, as reference.

For the evaluation of antimalarial therapies, the infection stage is also important (Díaz *et al.*, 2009). Only limited articles have addressed this problem (Díaz *et al.*, 2009; Ruberto *et al.*, 2002). Future work should focus on discrimination among different stages of malaria parasite, as well as different malaria species. The authors believe that the proposed approach will be capable of discrimination if trained appropriately.

Furthermore, malaria parasites from culture in medium were used for part of the development. As malaria parasites in patient's blood could have various conditions that effect the parasite morphology, future work should be done only on blood from malaria positive patients.

We conclude that our scanner is an easy-to-use and fast solution to detect low parasite densities in peripheral blood samples, without requiring a skilled microscopist or a wet lab. Our system shows superior performance compared to relevant alternative proposals in the literature.

Acknowledgements

The authors would like to thank Jan van Beek, Ivo Camps, Albert Geven, Nicole Haex, David Halter, Frank Jaartsveld, Frank Kneepkens, Michael Maris, Caroline Santamaria, Jean Sleipen, Nico Willard, Ton Wismans and Rien van Leeuwen for their contributions and fruitful discussions.

Parasites were kindly provided by Radboud University Nijmegen. We thank Prof. Robert Sauerwein and Marga van de Vegte.

We would like to thank the staff and patients at Chittagong Medical College Hospital and our colleagues in Bangladesh who facilitated the collection of patient material, in particular Md Amir Hossain, Md Abu Sayeed, Aniruddha Ghose, Abdullah Abu Sayeed and M. Abul Faiz.

The testing with patient material in Bangladesh was made possible by the kind support of Prof. Arjen Dondorp.

References

Bell, D. & Peeling, R. (2006) Evaluation of rapid diagnostic tests: malaria. *Nat. Rev. Microbiol.* **4**, S34–S38.

Camps, I.G.J., Laubscher, M., Peeters, E., Piciu, O.M., Willard, N.P. & Wimberger-Friedl, R. (2012) Preparation of thin layers of a fluid containing cells for analysis. US-Patent: US20120225446A1.

Coleman, R., Sattabongkot, J., Promstaporm, S., *et al.* (2006) Comparison of pcr and microscopy for the detection of asymptomatic malaria in a plasmodium falciparum/vivax endemic area in thailand. *Malar. J.* **5**, 121.

Díaz, G., González, F.A. & Romero, E. (2009) A semi-automatic method for quantification and classification of erythrocytes infected with malaria parasites in microscopic images. *J. Biomed. Inform.* **42**, 296–307.

Frean, J. (2009) Reliable enumeration of malaria parasites in thick blood films using digital image analysis. *Malar. J.* **8**, 218.

Freund, Y. & Schapire, R.E. (1996) Experiments with a new boosting algorithm. In *Proceedings of the 13th International Conference on Machine Learning*, pp. 148–156. Bari, Italy

Freund, Y. & Schapire, R.E. (1997) A decision-theoretic generalization of on-line learning and an application to boosting. *J. Comput. Syst. Sci.* **55**, 119–139.

Haralick, R.M. & Shapiro, L.G. (1992) *Computer and Robot Vision*. 1st edn. Addison-Wesley Longman Publishing Co., Inc., Boston, MA.

Hare, J.D. & Bahler, D.W. (1986) Analysis of *Plasmodium falciparum* growth in culture using acridine orange and flow cytometry. *J. Histochem. Cytochem.* **34**, 215–220.

He, Z., Tan, T. & Sun, Z. (2010) Topology modeling for adaboost-cascade based object detection. *Pattern Recognit. Lett.* **31**, 912–919.

Houwen, B. (2002) Blood film preparation and staining procedures. *Clin. Lab. Med.* **22**, 1–14.

Jain, A. & Chandrasekaran, B. (1982) Dimensionality and sample size considerations in pattern recognition practice. *Classification Pattern Recognition and Reduction of Dimensionality* vol. 2 of *Handbook of Statistics*. pp. 835–855. Elsevier, Amsterdam, The Netherlands.

Jain, A., Duin, R. & Mao, J. (2000) Statistical pattern recognition: a review. *IEEE Trans. Pattern Anal. Mach. Intell.* **22**, 4–37.

Keiser, J., Utzinger, J., Premji, Z., Yamagata, Y. & Singer, B.H. (2002) Acridine orange for malaria diagnosis: its diagnostic performance, its promotion and implementation in tanzania, and the implications for malaria control. *Ann. Trop. Med. Parasitol.* **96**, 643–654.

McQueen, P. & McKenzie, F. (2004) Age-structured red blood cell susceptibility and the dynamics of malaria infections. *Proc. Natl. Acad. Sci. U.S.A.* **101**, 9161–9166.

Moody, A. (2002) Rapid diagnostic tests for malaria parasites. *Clin. Microbiol. Rev.* **15**, 66–78.

Ruberto, C.D., Dempster, A.G., Khan, S. & Jarra, B. (2002) Analysis of infected blood cell images using morphological operators. *Image Vis. Comput.* **20**, 133–146.

Sezgin, M. & Sankur, B. (2004) Survey over image thresholding techniques and quantitative performance evaluation. *J. Electr. Imag.* **13**, 146–168.

Sio, S.W.S., Sun, W., Kumar, S., *et al.* (2007) Malariacount: an image analysis-based program for the accurate determination of parasitemia. *J. Microbiol. Method.* **68**, 11–18.

Špringl, V. (2009) *Automatic malaria diagnosis through microscopy imaging*. Master's Thesis, Center for Machine Perception, K13133 FEE Czech Technical University Prague, Czech Republic.

Stan, S.G. (1998) *The CD-ROM Drive: A Brief System Description*. Kluwer Academic Publishers, Norwell, MA.

Tek, F., Dempster, A. & Kale, I. (2009) Computer vision for microscopy diagnosis of malaria. *Malar. J.* **8**, 153.

Toha, S. & Ngah, U. (2007) Computer aided medical diagnosis for the identification of malaria parasites. In *Proceedings of the International Conference on Signal Processing, Communications and Networking.* pp. 521–522. Chennai, India.

Vink, J.P. & de Haan, G. (2011) No-reference metric design with machine learning for local video compression artifact level. *IEEE J. Select. Topics Signal Process.* **5**, 297–308.

Vink, J.P. & de Haan, G. (2012) Comparison of machine learning techniques for target detection. *Artif. Intell. Re*. Available at: http://link.springer.com/article/10.1007/s10462-012-9366-7. Accessed November 2012.

Viola, P. & Jones, M.J. (2001) Robust real-time object detection. *In Proceedings of the Second International Workshop on Statistical and Computational Theories of Vision Modeling, Learning, Computing and Sampling*, pp. 149–154, Vancouver, Canada.

Viola, P. & Jones, M. J. (2004) Robust real-time face detection. *Int. J. Comput. Vis.* **57**, 137–154.

Weszka, J.S., Dyer, C.R. & Rosenfeld, A. (1976) A comparative study of texture measures for terrain classification. *IEEE Trans. Syst., Man Cybernet.* **SMC-6**, 269–285.

WHO (2010a) *Basic Malaria Microscopy Part I: Learner's Guide*. WHO Press, Geneva.

WHO (2010b) *World Malaria Report 2010*. WHO Press, Geneva.

WHO (2011) *Malaria rapid diagnostic test performance—results of WHO product testing of malaria RDTs: round 3 (2010-2011)*. World Health Organization, Geneva.

Zhou, M. (2008) *Gabor-boosting face recognition*. PhD Thesis, School of Systems Enigneering, University of Reading.